

Model-independent reconstruction of the linear anisotropic stress η

Ana Marta Pinho^a Santiago Casas^{a,b} Luca Amendola^a

^aI TP, Ruprecht-Karls-Universität Heidelberg
Philosophenweg 16, 69120 Heidelberg, Germany

^bAIM, CEA, CNRS, Université Paris-Saclay, Université Paris Diderot,
Sorbonne Paris Cité, F-91191 Gif-sur-Yvette, France

E-mail: pinho@thphys.uni-heidelberg.de, santiago.casas@cea.fr,
amendola@thphys.uni-heidelberg.de

Abstract. In this work, we use recent data on the Hubble expansion rate $H(z)$, the quantity $f\sigma_8(z)$ from redshift space distortions and the statistic E_g from clustering and lensing observables to constrain in a model-independent way the linear anisotropic stress parameter η . This estimate is free of assumptions about initial conditions, bias, the abundance of dark matter and the background expansion. We denote this observable estimator as η_{obs} . If η_{obs} turns out to be different from unity, it would imply either a modification of gravity or a non-perfect fluid form of dark energy clustering at sub-horizon scales. Using three different methods to reconstruct the underlying model from data, we report the value of η_{obs} at three redshift values, $z = 0.29, 0.58, 0.86$. Using the method of polynomial regression, we find $\eta_{\text{obs}} = 0.57 \pm 1.05$, $\eta_{\text{obs}} = 0.48 \pm 0.96$, and $\eta_{\text{obs}} = -0.11 \pm 3.21$, respectively. Assuming a constant η_{obs} in this range, we find $\eta_{\text{obs}} = 0.49 \pm 0.69$. We consider this method as our fiducial result, for reasons clarified in the text. The other two methods give for a constant anisotropic stress $\eta_{\text{obs}} = 0.15 \pm 0.27$ (binning) and $\eta_{\text{obs}} = 0.53 \pm 0.19$ (Gaussian Process). We find that all three estimates are compatible with each other within their 1σ error bars. While the polynomial regression method is compatible with standard gravity, the other two methods are in tension with it.

Keywords: Model-independent approach - Cosmology - Gravity

ArXiv ePrint: [arXiv:1805.00027](https://arxiv.org/abs/1805.00027)

Contents

1	Introduction	1
2	Model-independent observables	2
3	Data	5
3.1	Hubble parameter data	6
3.2	E_g data	7
3.3	$f\sigma_8$ data	7
4	Reconstruction of functions from data	8
4.1	Binning	8
4.2	Gaussian Process	9
4.3	Polynomial regression	11
5	Results	12
6	Conclusions	15
A	The impact of the H_0 choice	17
B	Subtleties of the Gaussian Process method	19
C	Details of the Polynomial Regression Method for the reconstruction of η_{obs}	19

1 Introduction

The recent observation of gravitational waves from a neutron star merger GW170817 by the LIGO/VIRGO collaboration together with its electromagnetic counterpart GRB170817 observed immediately afterwards by several telescopes around the world [1–5], placed very tight constraints on the difference between the speed of gravitational waves c_T and the speed of light c , constraining it to be fractionally smaller than 10^{-15} [1]. Consequences of such measurement (as for instance discussed in [6, 7]) include ruling out a sector of Horndeski’s theory [8–12], that is the most general theory of a single scalar field having only second order equations of motion and being free of ghost instabilities [13]. However, to rule out these sectors of the Horndeski Lagrangian one has to assume no extreme fine-tuning, the absence of attractors (see e.g. [14]), and a universal coupling between matter and the scalar field. Even after the c_T constraint, therefore, the Horndeski Lagrangian remains the most interesting extension of Einstein’s gravity to test in cosmology.

In the general Horndeski theory, and also in bimetric gravity [15], one can show that the gravitational slip, defined as the ratio of the gravitational potentials $\eta = -\Phi/\Psi$, has a relatively simple functional form in Fourier space

$$\eta = h_2 \frac{1 + h_4 k^2}{1 + h_5 k^2}, \quad (1.1)$$

with coefficients h_i which are free functions of time and depend on the four free functions appearing in the Horndeski Lagrangian [16–18]. The constraint from gravitational waves sets h_2 equal to 1 since $h_2 = 1/c_T^2$ [16], but leaves free all the other functions. In the limit of large (but still sub-horizon) scales and provided that the theory does contain at least one mass scale besides the Planck mass [19], one obtains $\eta = 1$. In all other cases, $\eta \neq 1$ signals a deviation from standard gravity or a form of dark matter that cannot be approximated by a perfect fluid.

Considering model-independent observables and linear structure formation, and assuming gravity remains universally coupled also when modified, one can build an estimate of η formed by three directly observable functions of redshift which we denote $E(z)$, $P_2(z)$ and $P_3(z)$ (see [20]). They will be defined in detail in the following section. The first function, $E(z)$, is the dimensionless Hubble function. The second one, $P_2(z)$, is equivalent to the $E_G(z)$ statistics [21], that depends on the lensing potential and on the growth rate of structure formation. Finally, $P_3(z)$ (introduced in [16]) is related to the derivative of $f\sigma_8(z)$, which is the growth rate of matter density perturbations times the normalization of the power spectrum. This is measured by galaxy clustering using redshift space distortions.

In order to reconstruct $E(z)$, $P_2(z)$ and $P_3(z)$, we use the most recent data available for $H(z)$ obtained with Type Ia Supernovae and cosmic chronometers, while for $f\sigma_8(z)$ and E_G we employ redshift space distortion and galaxy-galaxy lensing data from several collaborations, listed below in section 3.

The problem of reconstructing an unknown function and its derivative from sparse and noisy data is not trivial and it is an important task in all areas of science. In this work, we use three different strategies to estimate the unknown functions and their derivatives from the data. As the first method, we use a simple binning formalism, in which we group the available data in redshift bins and use discrete finite differences to compute the derivatives at the corresponding redshifts. This method suffers from strong numerical uncertainties since the derivatives are very sensitive to the binning size and the method cannot capture high-frequency modes in the data. The second one is the Gaussian Process method, a generalization of a Gaussian distribution, where instead of random variables, one has a distribution of random functions, connected by a specific correlation function. This method has been used several times in cosmology, especially for the determination of the equation of state of dark energy w and the Hubble function $H(z)$ (see [22–26]). The third method consists of a polynomial regression (used for example recently in [27]), in which one assumes a linear model for the underlying function. Using the so-called *normal equation*, we reconstruct the coefficients of the polynomial, which represents our continuous interpolation function of the data, which is later evaluated at specific redshifts.

In section 2 we explain the theoretical foundations of the determination of η . Section 3 describes the data used in our analysis and their processing before we apply our three reconstruction methods which are explained in section 4. The estimation of the gravitational slip and overall discussion of our results can be found in section 5. Finally, we present some of the caveats of the methods and suggest ways to improve this analysis with future work.

2 Model-independent observables

The geometry of the Universe can be well described by small scalar perturbations around a flat FLRW metric $ds^2 = -(1 + 2\Psi)dt^2 + a(t)^2(1 + 2\Phi)d\mathbf{x}^2$, with scale factor a and two scalar gravitational potentials Ψ and Φ . Using Einstein’s field equations and a pressureless perfect

fluid for matter, we can derive the two Poisson equations in Fourier space

$$-k^2(\Psi - \Phi) = 4\pi GH(z)^{-2}\Sigma(k, z)\rho_m(z)\delta_m(z, k) \quad (2.1)$$

$$-k^2\Psi = 4\pi GH(z)^{-2}\mu(k, z)\rho_m(z)\delta_m(z, k) \quad (2.2)$$

where z is the redshift, k the scale in terms of the cosmological horizon (the comoving scale k_{com} divided by aH), ρ_m is the background average matter density of the Universe, δ_m the matter density contrast and Σ and μ are two functions of scale and time which quantify the departure from standard gravity. In Einstein's General Relativity, these functions reduce to $\Sigma = 2$ and $\mu = 1$. The gravitational slip η is defined as the ratio between the two gravitational potentials

$$\eta = -\Phi/\Psi, \quad (2.3)$$

where the perturbation variables are considered to be the root-mean-squares of the corresponding random variables. Taking the appropriate ratios of the Poisson equations (Eq. 2.1 and Eq. 2.2) defined above, we find a simple relation for the modified lensing parameter: $\Sigma = \mu(1 + \eta)$. If we make no assumptions about the initial conditions of the Universe, neither on the primordial power spectrum, nor on the nature of dark matter or the details of galaxy bias, we cannot determine the matter background density nor the matter overdensity in a model-independent way (see [16]). Therefore, a quantity like $\mu(k, z)$ in modified gravity cannot be estimated without first assuming a model. However, one can define model-independent observable quantities which do not depend on the aforementioned assumptions. Following [20], these variables are called A , R , L and E , respectively denoting amplitude, redshift-space distortions, lensing, and the dimensionless Hubble function. They are defined as

$$\begin{aligned} A &= b\delta_m, & R &= f\delta_m, \\ L &= \Omega_{m0}\Sigma\delta_m, & E &= H/H_0. \end{aligned} \quad (2.4)$$

where b is the galaxy-matter linear bias, $f = \delta'_m/\delta_m$ is the growth rate where the prime is derivative with respect to $\ln a$, and Ω_{m0} is today's matter fractional density. Both f and b can be in general time- and space-dependent. The formalism below can be applied also in this case, but since the available data do not provide the space dependence, in the following we will assume that it can be ignored. For the same reason, also η will be assumed to be independent of scale in the observed range. Looking at Eq. (1.1), one sees that scale-independence sets in either at small scales $k \gg 1$, or at large scales $k \ll 1$ (but in this case $\eta \rightarrow 1$) or at all scales if $h_4 = h_5$ or if the theory does not contain a mass scale.

With the definitions (2.4), it was shown in [16, 20] that one can obtain three quantities which are model-independent and cancel out the effects of the shape of the primordial power spectrum and the galaxy bias, namely

$$P_1 \equiv \frac{R}{A} = \frac{f}{b}, \quad (2.5)$$

$$P_2 \equiv \frac{L}{R} = \frac{\Omega_{m0}\Sigma}{f}, \quad (2.6)$$

$$P_3 \equiv \frac{R'}{R} = f + \frac{f'}{f} = \frac{(f\sigma_8(z))'}{f\sigma_8(z)}. \quad (2.7)$$

We have defined $f\sigma_8(z)$ as

$$f\sigma_8(z) = \sigma_8 G(z) f(z), \quad (2.8)$$

where σ_8 is the amplitude of the linear power spectrum defined in a spherical shell of radius 8 Mpc at redshift $z = 0$ and $G(z)$ is the growth function normalized to unity today, $\delta(z) = \delta_{m,0}G(z)$.

Together with the continuity equation and the Euler equation, relating the divergence θ of the peculiar velocities of galaxies propagating on geodesics to the gravitational potential Ψ

$$(a^2\theta)' = a^2k^2H\Psi \quad (2.9)$$

we can write down the lensing and Poisson equations in Fourier space, respectively, in the following way

$$-k^2(\Psi - \Phi) = \frac{3(1+z)^3L}{2E^2} \quad (2.10)$$

$$-k^2\Psi = R' + R\left(2 + \frac{E'}{E}\right). \quad (2.11)$$

This last equation is usually known as the equation of linear growth of matter perturbations. Dividing the lensing equation Eq. (2.10) by the equation for the growth of structure Eq. (2.11), we can obtain the ratio of the gravitational potentials and therefore the gravitational slip as a function of model-independent observables

$$\eta_{\text{obs}} \equiv \frac{3P_2(1+z)^3}{2E^2\left(P_3 + 2 + \frac{E'}{E}\right)} - 1 = \eta. \quad (2.12)$$

In order to distinguish the observables from the theoretical expectations, we denoted the combination on the left-hand-side of this equation as η_{obs} . This is the quantity we will reconstruct using present data in a model-independent way. As advertised, η_{obs} is independent of the initial power spectrum, of the bias, of the density of matter, and of assumptions about the cosmic expansion (that is, we do not require a Λ CDM background or any other).

The parameter P_2 can be related to the E_g statistics, defined in the cosmological literature (see [21] and references therein) as the expectation value of the ratio of lensing and galaxy clustering observables at a scale k

$$E_g = \left\langle \frac{a\nabla^2(\Psi - \Phi)}{3H_0^2 f \delta} \right\rangle_k. \quad (2.13)$$

Using the Poisson equation (2.1) and the definition of the A , R , L , E variables (Eq. 2.4), the relation with P_2 is simply given by

$$P_2 = 2E_g. \quad (2.14)$$

As we will mention in the next section, the available estimates of E_g reduce to P_2 only under some conditions. The E_g statistics has been used several times as a test of modified gravity ([28], [21], [29]). However, it is not *per se* a model-independent test. In fact, the theoretical value of E_g depends on Ω_{m0} and on f . Nevertheless, Ω_{m0} is not an observable quantity. Distance indicators, for instance Supernovae or BAO, measure $H(z)$ or its integral. To estimate the matter fraction Ω_{m0} given $H(z)$, one needs to assume that “matter” goes like a^{-3} and the rest is parametrized by an equation of state with few parameters. In modified gravity models, neither is necessarily true. More in general, the “dark degeneracy” discussed for instance in [30] shows that the separation between a matter component and a dark energy component is unavoidably model dependent. There is a second problem with

E_g , namely the fact that the growth rate f is estimated by solving the differential equation of the perturbation growth. This requires initial conditions, that are normally taken to be pure CDM at high redshift (this is for instance how the well-known approximated formula $f \approx \Omega_m^\gamma(z)$ is obtained). Again, this assumption is not necessarily true in modified gravity, as for example it is not true in the original Brans-Dicke model. As a consequence of this, when we compare E_g to the observed value, we can never know whether any discrepancy with respect to Λ CDM and standard gravity is due to a different value of Ω_{m0} or different initial conditions, or it is a genuine signature of a non-standard modified gravity parameter Σ . So E_g can be employed to test specific models, e.g. a Λ CDM expansion in standard gravity – a very important task, indeed – but not to measure directly the properties of gravity. In contrast, the statistics η_{obs} of Eq. (2.12) is model-independent because it estimates directly η without any need to assume a value of Ω_{m0} nor to assume initial conditions for f . Thus, if observationally one finds $\eta_{obs} \neq 1$, then Λ CDM and all the models in standard gravity and in which dark matter is a perfect fluid are ruled out. Finally, we notice that in [31] a cautionary remark is pointed out, namely that their results about E_g cannot be employed until the tension between Ω_{m0} in different observational datasets is resolved. This problem does not arise with η_{obs} .

Eq. (2.12) is a model-independent estimate of η that depends purely on observable quantities. As we already mentioned, the prefactor h_2 in Eq. (1.1) is directly related to c_T , so that for $c_T = c$, h_2 is equal unity. This means that at large enough scales (for $k \rightarrow 0$), $\eta \rightarrow 1$ and one has the consistency relation

$$3P_2(1+z)^3 = 4E^2 \left(P_3 + 2 + \frac{E'}{E} \right). \quad (2.15)$$

However, these large scales should still be sub-sound-horizon, so that the quasi-static limit applies; moreover, the limit will actually be different from unity in models without a mass scale, see e.g. [19]. Therefore, in practice, this large-scale consistency relation is not particularly useful and we will not discuss it any longer.

3 Data

In this work we reconstruct $E(z)$, $P_2(z)$ and $P_3(z)$ using the data listed in Tables 3, 5, 6, 4, 7 and 8, which are also shown in figure 1. We use Hubble parameter data to obtain $E(z)$ and $E'(z)$. For $P_2(z)$ we apply a simple rescaling of $E_g(z)$ data, while $P_3(z)$ is reconstructed from $f\sigma_8(z)$ and its derivative with respect to $\ln a$. We show in Table 1 the cosmological parameters from the TT+TE+EE+lowE+lensing Planck 2018 best-fits [32], that we use to plot the Λ CDM curves of different cosmological functions in figure 1. The details of the sources of the data will be explained below.

Ω_{m0}	Ω_{DE}	Ω_b	n_s	σ_8	$H_0[\text{km/s/Mpc}]$
0.3153	0.6847	0.0493	0.9649	0.8111	73.45

Table 1. Fiducial parameter values for our reference Λ CDM case, using Planck 2018 data from TT+TE+EE+lowE+lensing [32], except for H_0 , where we use the local value from the HST collaboration [33] as explained on the main text.

For the results of this work, we only use the H_0 value to normalize $H(z)$ measurements into the dimensionless quantity $E(z)$. Notice that H_0 , contrary to Ω_{m0} , is an observable

quantity that can be estimated from local kinematics in a way which is independent of cosmology and modified gravity. Therefore, for the normalization of the $E(z)$ measurements we need to choose a value of H_0 , for instance from the recent results of the Planck collaboration [32] or the value obtained by the HST collaboration [33].

In this work, we choose the local value of H_0 determined by the HST collaboration [33] which amounts to $H_0^{HST} = 73.45 \pm 1.66$ [km/s/Mpc], because it is cosmology-independent. In Appendix A we discuss the results using the Planck value. Thus, by construction, we have an extra data point at $z = 0$, namely, $E(z = 0) = 1$. The uncertainty on H_0 propagates to all $E(z)$ values, and we take this into account as detailed in the next section.

3.1 Hubble parameter data

Regarding the Hubble parameter measurements, we have used the most recent compilation of $H(z)$ data from [23] (see Table 3), including the measurements from [34–37], Baryon Oscillation Spectroscopic Survey (BOSS) ([38–40]) and the Sloan Digital Sky Survey (SDSS) ([41], [42]).

In this compilation, the majority of the measurements was obtained using the cosmic chronometric technique, labeled as method 1 in Table 3. This method infers the expansion rate dz/dt by taking the difference in redshift of a pair of passively-evolving galaxies. The remaining measurements were obtained through the position of the Baryon Acoustic Oscillation (BAO) peaks in the power spectrum of a galaxy distribution for a given redshift. This is labeled as method 2 in Table 3.

In addition to these, we use the recent results from [43] where a compilation of Supernovae Type Ia from CANDELS and the CLASH *Multi-cycle treasury program* was analyzed, providing six measurements of the expansion rate $E(z)$, with considerably smaller error bars, compared to the other above mentioned techniques. These are listed on Table 4. In the original reference [43], the errors are not symmetric, therefore we recalculated symmetric errors, as the quadrature of the 1σ bounds on the left and right side of the central value.

The measurements from [38] and [39] are obtained using the BAO signal in the Lyman- α forest distribution alone or cross correlated with Quasi-Stellar Objects (QSO) (for the details of the observational methods, we refer the reader to the original papers). Reference [42] provides the covariance matrix of its three $H(z)$ measurements obtained from the radial BAO galaxy distribution. We report the covariance matrix on Table 5. To this compilation we add the results from the WiggleZ Dark Energy Survey [44] whose covariance matrix can be found on Table 6.

The measurements of H_0 obtained with the cosmic chronometric technique are independent of large-scale cosmology and recent work [24] has shown that these data prefer a lower value for the H_0 value. However, an upper value can also be found if a different model for the processing of the galaxies spectra is chosen when using the data from [40]. For our fiducial results, we fix our choice of the Hubble parameter to the HST measurement.

As previously mentioned, the data points of the Hubble parameter $H(z)$ have to be converted into the dimensionless expansion rate $E(z)$ by dividing by H_0 , since we need $E(z)$, a model-independent observable. For each measurement $H_i = H(z_i)$, we form

$$E_i = \frac{H_i}{H_0} \quad (3.1)$$

so that the error reads

$$\delta E_i = \frac{\delta H_i}{H_0} - H_i \frac{\delta H_0}{H_0^2}. \quad (3.2)$$

The covariance of this random matrix is then the expected value of the product of δE_i and δE_j , which is

$$\begin{aligned}\langle \delta E_i \delta E_j \rangle &= \left\langle \frac{\delta H_i}{H_0} \frac{\delta H_j}{H_0} \right\rangle + H_i H_j \left\langle \frac{\delta H_0}{H_0^2} \frac{\delta H_0}{H_0^2} \right\rangle \\ &= \frac{C_{ij}^{(H)}}{H_0^2} + E_i E_j \frac{(\sigma(H_0))^2}{H_0^2},\end{aligned}\tag{3.3}$$

where we have used the fact that errors on H_0 and H_i are uncorrelated, therefore $\langle \delta H_0 \delta H_i \rangle = 0$, $C_{ij}^{(H)}$ is the covariance matrix of our data on the Hubble function $H(z)$ and $\sigma(H_0)$ is the error on H_0 . Equation 3.3 amounts to adding an extra covariance matrix to our standard data covariance matrix.

3.2 E_g data

We use the E_g data compiled on Table 7. This compilation includes the results from KiDS+2dFLenS+GAMA [31], i.e, a joint analysis of weak gravitational lensing, galaxy clustering and redshift space distortions. We also include image and spectroscopic measurements of the Red Cluster Sequence Lensing Survey (RCSLenS) [45] where the analysis combines the the Canada-France-Hawaii Telescope Lensing Survey (CFHTLenS), the WiggleZ Dark Energy Survey and the Baryon Oscillation Spectroscopic Survey (BOSS). Finally the results of the VIMOS Public Extragalactic Redshift Survey (VIPERS) [28] is also accounted for in our data. They use redshift-space distortions and galaxy-galaxy lensing.

These sources provide measurements in real space within the scales $3 < R_p < 60 h^{-1} \text{Mpc}$ and in the linear regime, which is the one we are interested in. They have been obtained over a relatively narrow range of scales λ meaning that we can consider them relative to the $k = 2\pi/\lambda$ -th Fourier component, as a first approximation. In any case, the discussion about the k -dependence of η is beyond the scope of this work, so the final result can be seen as an average over the range of scales effectively employed in the observations. Moreover, in the estimation of E_g , based on [21], one assumes that the redshift of the lens galaxies can be approximated by a single value. With these approximations, indeed E_g is equivalent to $P_2/2$, otherwise E_g represents some sort of average value along the line of sight. We caution that these approximations can have a systematic effect both on the measurement of E_g and on our derivation of η . In a future work we will quantify the level of bias possibly introduced by these approximations in our estimate. For further details and discussion, see reference [45] and [28].

3.3 $f\sigma_8$ data

In order to calculate the variable P_3 , we need to reconstruct $f\sigma_8(z)$ and its derivative as a function of redshift. A compilation of the available data for $f\sigma_8(z)$ can be found in Table 8. This quantity can be obtained through measurements of the redshift-space distortions (RSD) in the two point-correlation function of a galaxy survey.

Our data includes measurements from the 6dF Galaxy Survey [46], the Subaru FMOS galaxy redshift survey (FastSound) [47], WiggleZ Dark Energy Survey [44], VIMOS-VLT Deep Survey (VVDS) [48], VIMOS Public Extragalactic Redshift Survey (VIPERS) [28, 49–51] and the Sloan Digital Sky Survey (SDSS) [42, 52–58]. Other works in the literature which perform RSD measurements, but only report $f\sigma_8(z)$ values indirectly, such that we have to assume something on the bias or on the σ_8 relation, e.g. [59] and [60], will not be considered

for our purposes. Furthermore, for numerical reasons, before applying any reconstruction method, we will use these data taking the natural logarithm, i.e. $\ln f\sigma_8(z)$, which allows us to compute the P_3 observable as a simple derivative with respect to $\ln a$.

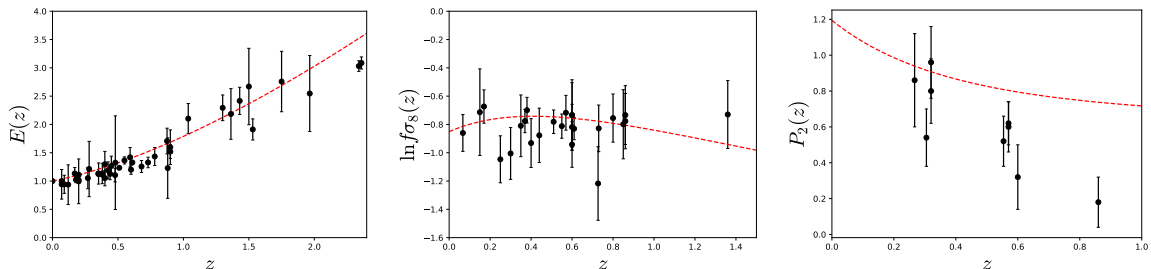


Figure 1. Data sets used in this work (black dots with error bars), plotted together with the corresponding reference Λ CDM prediction as a function of redshift (solid red line), using a Planck 2018 cosmology as reported on Table 1. **Left panel:** $E(z)$ data from Table [23]. We used the value of H_0 from the HST collaboration to rescale part of the data points from $H(z)$ to $E(z)$ (see main text). **Central panel:** Plot of the natural logarithm of the $f\sigma_8$ data points from Table 8. **Right panel:** Data set for P_2 , obtained using E_g data from Table 7. For $z > 0.5$ we see a large discrepancy between Λ CDM and the data points, which was also noted in [31].

4 Reconstruction of functions from data

The main difficulties in obtaining η_{obs} is that we need to take the ratios P_2 and P_3 at the same redshift, while we have datapoints at different redshifts, and that we need to take derivatives of $E(z)$ and $f\sigma_8(z)$. This essentially means we need to have a reliable way to interpolate the data to reconstruct the underlying behavior.

There is no universally accepted method to interpolate data. Depending on how many assumptions one makes regarding the theoretical model, e.g. whether the reconstructed functions need just to be continuous, or smooth, depending on few or many parameters, etc., one gets unavoidably different results, especially in the final errors. Here, we consider and compare three methods to obtain the value of η_{obs} : binning, Gaussian Process, and generalized polynomial regression.

4.1 Binning

One intuitive way to perform data reconstruction is to assemble the data into bins. This consists in dividing the data into particular redshift intervals and, for each of these intervals (bins), calculating the average of the data contained in that bin. Denoting $s_k \equiv s(z_k)$ as a generic data value, with dependent variable s , located at the point z_k with error σ_k^s , the binning procedure is done by applying the following formula

$$\bar{s}_i = \frac{\sum_k^{N_i} s_k (\sigma_k^s)^{-2}}{\sum_k^{N_i} (\sigma_k^s)^{-2}}, \quad \sigma_i^{\bar{s}} = \frac{1}{\sqrt{\sum_k^{N_i} (\sigma_k^s)^{-2}}} . \quad (4.1)$$

where N_i is the number of data points inside the bin i , \bar{s}_i is the new value of the dependent variable at the center of the bin z_i , where $z_i = (z_{k+1} - z_k)/2$ is simply the arithmetic mean between the upper and lower borders of the bin. The new error at this point is $\sigma_i^{\bar{s}}$. This means that we are converting the information of the subset of data contained in a specific

bin into one unique data point by taking the weighted average for the data values and the data errors over all points contained in that interval. The square of the new error bar at the center of the bin, namely $(\sigma_i^{\bar{s}})^2$, is then the mean of the errors squared from all the N_i points contained in the bin with index i .

To reconstruct our main observable η_{obs} , we also need to compute the derivatives of the data for the functions $E(z)$ and $\ln(f\sigma_8(z))$, at the exact same redshifts as for the other functions. Therefore, we need to bin the original data in alternative bins centered at new points z_j , so that using finite differences we can compute the derivative of the dependent variable and its associated error at the z_i in the following form

$$\bar{s}'_i = -(1 + z_i) \frac{\bar{s}(z_{j+1}) - \bar{s}(z_j)}{\Delta z_j}, \quad \sigma_i^{\bar{s}'} = (1 + z_i) \frac{1}{\Delta z_j} \sqrt{(\sigma_{j+1}^{\bar{s}})^2 + (\sigma_j^{\bar{s}})^2} \quad . \quad (4.2)$$

where $\Delta z_j = z_{j+1} - z_j$ and remembering that a prime denotes a derivative with respect to $\ln a$.

Our observable η_{obs} is estimated as in Eq. (2.12) through $E(z)$, P_2 , P_3 and $E'(z)$, which we will denote generally as $y^{(1)}$, $y^{(2)}$, $y^{(3)}$ and $y^{(4)}$, respectively. Consequently, to calculate the final error on η_{obs} , we use standard error propagation, assuming no correlation among the $y^{(i)}$ variables, so that the error $\sigma_i^{\eta_{\text{obs}}}$ at the redshift z_i is specifically

$$(\sigma_i^{\eta_{\text{obs}}})^2 = \sum_{\alpha=1}^4 \left(\sigma_i^{y^{(\alpha)}} \frac{\partial \eta_{\text{obs}}(z_i)}{\partial y^{(\alpha)}} \right)^2 \quad (4.3)$$

where we also assume that the bins are large enough, such that the correlation among the bins is negligible. In this way, Eq. (2.12) and its estimated error can be evaluated at the centers of the bins z_i . However, the maximum number of final bins N_i is constrained by the number of data points available for the smallest data set among the $y^{(\alpha)}$ functions. We will present results on the binning method with more detail in section 5.

4.2 Gaussian Process

Another way of reconstructing a continuous function from a dataset is using the method of Gaussian Process (see [61] for a comprehensive description). A Gaussian Process (GP) can be regarded as the generalization of Gaussian distributions to the space of functions, since it provides a probability distribution over continuous functions instead of a distribution over a random variable. Considering a dataset $\mathcal{D} = \{(x_i, y_i) | i = 1, \dots, n\}$ of n observables where x_i are deterministic variables and y_i random variables, the goal is to obtain a continuous function $f(x)$ that best describes the dataset. A function f evaluated at a point x is a Gaussian random variable with mean μ and variance $\text{Var}(f)$. The $f(x)$ values depend on the function value evaluated at another point x' . The relation between the value of the function at these two points can be given by a covariance function $\text{cov}(f(x), f(x')) = k(x, x')$, which evaluated at $x = x'$ gives the variance $\text{Var}(f(x)) = k(x, x)$. So, the distribution of functions at the point x is characterized by (for more details, see [22])

$$\mu(f(x)) = \mathcal{E}[f(x)] \quad k(x, x') = \mathcal{E}[(f(x) - \mu(x))(f(x') - \mu(x')))] \quad , \quad (4.4)$$

where \mathcal{E} is the expected value.

The covariance function $k(x, x')$ is in principle arbitrary. Since we are interested in reconstructing the derivative of the data, we need to chose a differentiable function. A

Gaussian covariance function

$$k(x, x') = \sigma_f^2 \exp \left[-\frac{(x - x')^2}{2\ell_f^2} \right] \quad (4.5)$$

is the covariance function that we choose in this work, as it is the most common and it has the least number of parameters. In the results section 5, we will discuss how this assumption does not change considerably our results. This function depends on the hyperparameters σ_f and ℓ_f , that allow to set the shape of the covariance function, which acts as a form of prior on the set of possible functions that we can obtain with the GP method. The hyperparameter ℓ_f can be considered as the typical correlation length scale of the independent variable, while the signal variance σ_f , can be thought of as the typical variation scale of the dependent variable.

In a Gaussian Process using real data (x_i, y_i) where $y_i = f(x_i) + \epsilon_i$, the errors are assumed to be Gaussian and the observations to be scattered around the underlying function. The noise ϵ_i is Gaussian with covariance matrix C , which needs to be taken into account for the joint likelihood function. This means that the reconstruction itself depends on the number and quality of data available.

Following a Bayesian approach, one can compute the joint likelihood function for the data and the reconstructed function. Thus, for a Gaussian prior for both the data and the random functions, one can marginalize over the space of functions f and obtain the logarithm of the marginal likelihood as (see [22])

$$\begin{aligned} \ln \mathcal{L} = & -\frac{1}{2} \sum_{i,j=1}^N \left\{ [y_i - \mu(x_i)] [k(x_i, x_j) + C(x_i, x_j)]^{-1} [y_j - \mu(x_j)] \right\} \\ & -\frac{1}{2} \ln |k(x_i, x_j) + C(x_i, x_j)| - \frac{N}{2} \ln 2\pi . \end{aligned} \quad (4.6)$$

Maximizing the logarithm of the marginal likelihood gives then the optimal hyperparameters σ_f and ℓ_f . In a full Bayesian approach, one should marginalize over the hyperparameters, using Monte Carlo Markov chain (MCMC) algorithms, in order to obtain the fully marginalized posterior distribution on the reconstructed function. As suggested in [22], we assume that the probability distribution of the hyperparameters is sharply peaked, which allows us to take them out of the integration and effectively fix them to their optimal values.

The Gaussian Process algorithm is implemented in a publicly available python code, named GaPP (Seikel et al. (2012) [22]). The GaPP code computes the continuous function of a given dataset and its derivatives up to third order, for a multi-dimensional dataset. It also takes into account correlated errors in the data and allows one to choose among different covariance functions, also known as kernel functions. For the case of the Gaussian kernel function as described above, the σ_f and ℓ_f parameters are optimized by the GaPP code through the maximization of the logarithm of the marginal likelihood function in Eq. (4.6).

Also, for the case of reconstructing the derivative of the data, a covariance between the reconstruction of f and f' arises, that should also be determined by a Monte Carlo sampling. GaPP takes a first order approximation and uses statistical error propagation which is valid for small errors. These approximations may have an impact on the final constraints of this work, particularly as underestimated errors on the reconstructed function as discussed on the original reference [22].

For each of the data sets, we will use the GaPP code to reconstruct the underlying function and its derivative where we did not specify any prior on the hyperparameters or

the mean function of the Gaussian Process to remain agnostic towards these choices. The details of our approach using this code concerning the chosen hyperparameters and covariance functions will be discussed in Section 5.

4.3 Polynomial regression

As a third reconstruction method, we use a generalized polynomial regression, a widely used method to obtain model parameters from data. Since we want to do this as model-independently as possible, we do not impose a priori any polynomial order for the reconstruction, but we let the data decide which is the maximum possible order. In the following we will describe the standard method of polynomial regression. Nevertheless, there are a number of complications due to the application to differentiated data with correlated errors, so that we will discuss the method in detail in App. C.

We start by assuming that we have N data points y_i , one for each value of the *independent* variable x_i (which are *not* random variables) and that

$$y_i = f_i + e_i \quad (4.7)$$

where e_i are errors (random variables) which are assumed to be distributed as Gaussian variables. Here f_i are theoretical functions that depend linearly on a number of parameters A_α

$$f_i = \sum_{\alpha} \bar{A}_{\alpha} g_{i\alpha} \quad (4.8)$$

where $g_{i\alpha}(x_i)$ are functions of the variable x_i . This is the definition of a linear model. Defining the matrix of basis functions as G and the data vector as D in the following way

$$G_{\alpha\beta} \equiv g_{\beta i} C_{ij}^{-1} g_{\alpha j} \quad (4.9)$$

$$D_{\alpha} \equiv y_i C_{ij}^{-1} g_{\alpha j} \quad (4.10)$$

(always summing over repeated Latin indexes), where C_{ij} is the data covariance matrix, we can see that the linear model can be written as

$$\mathbf{GA} = \mathbf{D} . \quad (4.11)$$

We are interested in finding the coefficients $\mathbf{A} = \{A_0, A_1, \dots\}$ of the model. To do so, we can invert the above equation to solve for \mathbf{A} as

$$\bar{\mathbf{A}} = \mathbf{G}^{-1} \mathbf{D} , \quad (4.12)$$

which is also known as the *normal equation*.

If the prior is uniform in an infinite range (improper prior), the parameters in the linear problem have a Gaussian posterior with mean $\bar{\mathbf{A}}$ and correlation matrix given by the inverse of its Fisher matrix. Since in the linear problem the data covariance matrix does not depend on the parameters, we have the following Fisher matrix

$$F_{\alpha\beta} \equiv C_{ij}^{-1} \frac{\partial f_i}{\partial A_{\alpha}} \frac{\partial f_j}{\partial A_{\beta}} = C_{ij}^{-1} g_{\alpha i} g_{\beta j} = G_{\alpha\beta} . \quad (4.13)$$

Once the coefficients are known, we can obtain the data values on a point x_A , which is not one of the points present in the data, using the expression in Eq. (4.8) and evaluating it at

x_A , namely $f_A = \sum_{\alpha} \bar{A}_{\alpha} g_{A\alpha}$, where $g_{A\alpha}$ means the function g_{α} evaluated at x_A , with an error $\sigma_A^2 = F_{\alpha\beta}^{-1} g_{A\alpha} g_{A\beta}$. We can select a number of arbitrary points $x_{A,B,C}$ and obtain the error matrix for the reconstructed function at these points as

$$C_{AB} = F_{\alpha\beta}^{-1} g_{A\alpha} g_{B\beta}. \quad (4.14)$$

In our particular case, we have three datasets $(y^{(0)}, y^{(1)}, y^{(2)}) = (\ln(f_{s8}(z)), E(z), E_G(z))$ and we wish to estimate the error on a function $\eta_{\text{obs}}(y^{(1)}, y^{(2)}, y^{(3)}, y^{(4)})$, where $y^{(4)} = y^{(1)'}$ and $y^{(3)} = y^{(0)'}$ where a prime denotes, as already mentioned, a derivative with respect to $\ln(a)$. We leave the details for App.C. The only issue we discuss here is the order of the polynomial. The order is of course in principle arbitrary, up to the number of data points for each data set. However, it is clear that with too many free parameters the resulting χ^2 will be very close to zero, that is statistically unlikely. At the same time, too many parameters also render the numerical Fisher matrix computationally unstable (producing, e.g., a non-positive definite matrix) and the polynomial wildly oscillating. On the other hand, too few parameters restrict the allowed family of functions. Therefore, we select the order of the polynomial function by choosing the polynomial degree for which the reduced chi-squared $\chi_{\text{red}}^2 = \chi^2/(N - P)$, is closest to 1 and such that the Fisher matrix is positive definite. Since our datasets contains data points from different experiments, there are some data points located at the same redshift or very close to each other, with different values of the dependent variable. In the case of a perfect fit, the polynomial would go through all points leading to spurious oscillations. For this reason, we take the weighted average of data points that are closer than $\Delta z = 0.01$ in redshift, before using them as an input into the polynomial regression algorithm.

5 Results

Let us now discuss the results of the final observable η_{obs} for each of these methods. The binning method contains the least number of assumptions compared to the polynomial regression or the Gaussian Process method. It is essentially a weighted average over the data points and its error bars at each redshift bin. Since we need to take derivatives in order to calculate P_3 and E' , and we have few data points, we opt to compute finite difference derivatives. This has the caveat that it introduces correlations among the errors of the function and its derivatives, that we cannot take into account with this simple method. Moreover, for the binning method, we do not take into account possible non-diagonal covariance matrices for the data, which we do for polynomial regression and the Gaussian Process reconstruction.

Figure 2 shows the reconstructed functions obtained by the binning method, the Gaussian Process and with polynomial regression, alongside with the theoretical prediction of the standard Λ CDM model. In all cases the error bars or the bands represent the 1σ uncertainty.

With the binning method, the number of bins is limited by the maximum number of existing data redshifts from the smallest data set corresponding to one of our model-independent observables. In this case, this is the quantity E_g , for which we have effectively only three redshift bins. Looking at Table 7 and comparing with Figure 1, we can see that there are nine E_g data points, but most of them are very close to each other in redshift, due to being measured by different collaborations or at different scales in real space for the same z . As explained in the data section above, we just regard this data as an average over different scales, assuming that non-linear corrections have been correctly taken into account by the respective experimental collaboration. Since we do not have to take derivatives of E_g ,

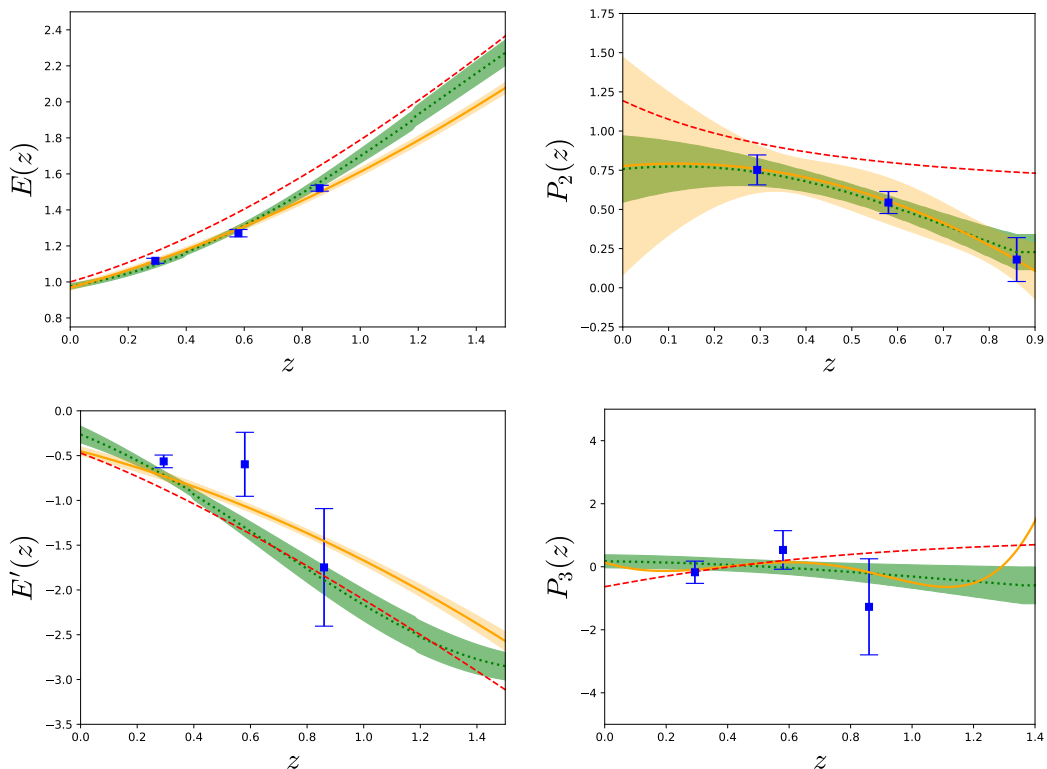


Figure 2. Comparison of the three reconstruction methods for each of the model-independent variables. The binning method in blue squares with error bars, Gaussian Process as a green dotted line with green bands, polynomial regression as a solid yellow line with yellow bands. All of them depicting the 1σ uncertainty. **Left panel:** Plot of the reconstructed $E(z)$ function on the top and its derivative $E'(z)$ on the bottom. **Right panel:** Plot of the reconstructed $P_2(z)$ function on the top and the reconstructed $P_3(z)$ function on the bottom. For each case, we show the theoretical prediction of our reference Λ CDM model as a red dashed curve.

or equivalently P_2 , this leaves us with three possible redshift bins, centered at $z_1 = 0.294$, $z_2 = 0.580$ and $z_3 = 0.860$, all of them with an approximate bin width of $\Delta z \approx 0.29$. At these redshifts we obtain $\eta_{\text{obs}}(z_1) = 0.48 \pm 0.45$, $\eta_{\text{obs}}(z_2) = -0.03 \pm 0.34$ and $\eta_{\text{obs}}(z_3) = -2.78 \pm 6.84$. These values and the estimation of the intermediate model-independent quantities can be seen in Table 2.

Regarding the Gaussian Process method, we have computed the normalized Hubble function and its derivative, $E(z)$ and $E'(z)$ with the *dgp* module of the GaPP code. Using the data of Table 4 and its correlation matrix, we reconstructed the $E(z)$ and $E'(z)$ for the redshift interval of the data using the Gaussian function as the covariance function and initial values of the hyperparameters $\theta = [\sigma_f = 0.5, \ell_f = 0.5]$ that later are estimated by the code. The same procedure was done for the $P_2(z)$ data, obtained by Eq. (2.14) using the Table 7. We obtain for $E(z)$ and $E'(z)$ functions the hyperparameters $\sigma_f = 2.12$ and $\ell_f = 2.06$ and for the P_2 function, $\sigma_f = 0.58$ and $\ell_f = 0.67$.

For the $P_3(z)$ observable, the hyperparameters obtained by the GaPP code led to a very flat and unrealistic reconstruction, that suggested us to take another approach for obtaining the optimal hyperparameters. More details can be found on Appendix B. We sampled the logarithm of the marginal likelihood on a grid of hyperparameters σ_f, ℓ_f from 0.01 to 2,

setting this way a prior with the redshift range of the dataset, and 300 points equally separated in log-space for each dimension. Remember that the hyperparameter ℓ_f constrains the typical scale on the independent variable z . Thus, as an additional prior, we impose that ℓ_f needs to be smaller than the redshift range of the data, which was not guaranteed by the default GaPP code. Then we chose the pair of hyperparameters corresponding to the maximum of the log-marginal likelihood Eq. (4.6). Therefore, for the $\ln(f\sigma_8(z))$ data, we obtain $\sigma_f = 0.549$ and $\ell_f = 1.361$. Its reconstructed derivative P_3 can be seen in the lower right panel of Figure 2. The function remains relatively flat, compared to the one given by other methods, but this approach has improved the determination of this observable, as further justified in Appendix B.

Regarding the choice of the kernel function, several functions were compared, each of them with a different number of parameters to see the impact on the output. We tested the Gaussian kernel with two parameters, (σ_f, ℓ_f) ; the rational quadratic kernel with three parameters and the double Gaussian kernel with four parameters (see the original reference for the explicit implemented formula [22]). We performed tests using the $H(z)$ data obtained with the cosmic chronometer technique and the $f\sigma_8(z)$ data. Our tests show that the different choices shift the reconstructed function up to 6% on its central value compared to the Gaussian kernel function. This happens for $H(z)$ while the effect is negligible for $f\sigma_8(z)$. Taking into account the above choices and procedure, we report that with the Gaussian Process method we obtain $\eta_{\text{obs}}(z_1) = 0.38 \pm 0.23$, $\eta_{\text{obs}}(z_2) = 0.91 \pm 0.36$ and $\eta_{\text{obs}}(z_3) = 0.58 \pm 0.93$.

Method	Parameter	Redshift bins			Weighted mean
		$z_1 = 0.294$	$z_2 = 0.58$	$z_3 = 0.86$	
Binning	$E(z)$	1.12 ± 0.01	1.27 ± 0.02	1.51 ± 0.02	0.15 ± 0.27
	$E'(z)$	-0.56 ± 0.07	-0.60 ± 0.36	-1.75 ± 0.66	
	$P_2(z)$	0.75 ± 0.10	0.54 ± 0.07	0.18 ± 0.14	
	$P_3(z)$	-0.17 ± 0.35	0.53 ± 0.61	-1.27 ± 1.52	
	$\eta_{\text{obs}}(z)$	0.48 ± 0.45	-0.03 ± 0.34	-2.78 ± 6.84	
Gaussian Process	$E(z)$	1.10 ± 0.01	1.30 ± 0.02	1.55 ± 0.03	0.53 ± 0.19
	$E'(z)$	-0.73 ± 0.05	-1.30 ± 0.10	-1.89 ± 0.16	
	$P_2(z)$	0.74 ± 0.09	0.53 ± 0.06	0.23 ± 0.11	
	$P_3(z)$	-0.10 ± 0.20	-0.03 ± 0.21	-0.21 ± 0.30	
	$\eta_{\text{obs}}(z)$	0.38 ± 0.23	0.91 ± 0.36	0.58 ± 0.93	
Polynomial Regression	$E(z)$	1.12 ± 0.01	1.29 ± 0.02	1.50 ± 0.02	0.49 ± 0.69
	$E'(z)$	-0.73 ± 0.04	-1.06 ± 0.04	-1.45 ± 0.04	
	$P_2(z)$	0.76 ± 0.15	0.55 ± 0.15	0.18 ± 0.14	
	$P_3(z)$	-0.09 ± 0.80	0.14 ± 0.78	-0.17 ± 3.02	
	$\eta_{\text{obs}}(z)$	0.57 ± 1.05	0.48 ± 0.96	-0.11 ± 3.21	

Table 2. The reconstructed or measured model-independent variables $E, E', P_2, P_3, \eta(z)$ at three different redshifts $z = (0.294, 0.58, 0.86)$, together with their 1σ errors, for each of the reconstruction methods. The polynomial regression method is compatible with the Λ CDM scenario while the other two methods show some tension at lower redshift.

For the polynomial regression method, we find $\eta_{\text{obs}}(z_1) = 0.57 \pm 1.05$, $\eta_{\text{obs}}(z_2) = 0.48 \pm 0.96$ and $\eta_{\text{obs}}(z_3) = -0.11 \pm 3.21$. Note that we applied the criteria of a χ_{red}^2 closest to one and a positive definite Fisher matrix to choose the order of the polynomial for each of the datasets. These criteria led to a choice of a polynomial of order 3 for the $E(z)$ and $E_g(z)$ data and order 6 for the $\ln(f\sigma_8(z))$ data. These polynomials can be seen in Figure 2 as solid yellow lines, together with their 1σ uncertainty bands. The higher order of the polynomial of $\ln(f\sigma_8(z))$ explains the "bumpiness" of the reconstruction of P_3 , leading to larger errors

on this observable in comparison to the GP method.

In Fig. 3 we show the reconstructed η_{obs} as a function of redshift with the three different methods, again with GP in a green dashed line, polynomial regression in a yellow solid line and the binning method in blue squares with error bars. It is possible to conclude that the methods are consistent with each other, within their 1σ uncertainties and that in most bins the results are consistent with the standard gravity scenario. We find that the error bars of the Gaussian Process reconstruction are generally smaller than the other methods, such that at the lowest redshift, GP is not compatible with $\eta_{\text{obs}} = 1$ at nearly 2σ , while in the case of the binning method at the intermediate redshift, $z = 0.58$, the tension is nearly 3σ .

As detailed in section 3.1, we need to choose a value of H_0 to obtain the dimensionless Hubble function $E(z)$. We tested that our results do not change significantly with a different choice of H_0 . The comparison between the value from the Planck 2018 collaboration and the HST collaboration is described on Appendix A.

Finally, we can combine the estimates at three redshifts of Table 2 into a single value. Assuming a constant η_{obs} in this entire observed range and performing a simple weighted average, we find finally $\eta_{\text{obs}} = 0.15 \pm 0.27$ (binning), $\eta_{\text{obs}} = 0.53 \pm 0.19$ (Gaussian Process) and $\eta_{\text{obs}} = 0.49 \pm 0.69$ (polynomial regression). The Gaussian Process method yields the smallest error and would exclude standard gravity. However, despite being sometimes advertised as “model-independent”, we believe that this method actually makes a strong assumption, since it compresses the ignorance about the reconstruction into a kernel function that depends on two or a small number of parameters, which are often not even fully marginalized over, as we did in our case. Also the binning method taken at face value would rule out standard gravity. However, as already mentioned, we did not take into account the correlation induced by the finite differences, and this might have decreased the overall error. Overall, we think the polynomial regression method is the most satisfactory one, providing the best compromise between the least number of assumptions and the best estimation of the data derivative. Therefore, we consider it as our “fiducial” result.

6 Conclusions

Large scale surveys like Euclid will soon allow to combine lensing and clustering data of unprecedented quality and quantity to probe gravity. To this aim, it is important to perform both null-tests of specific models, like Λ CDM, and to measure the properties of modified gravity in a way that does not depend on too many assumptions.

One of the clearest way to test gravity is to estimate the anisotropic stress η , defined as the ratio of the time-time and the space-space metric linear potentials Φ, Ψ . A value of $\eta \neq 1$ would signal a modification of gravity (for instance, a fifth force induced by a scalar field) or the presence of a relativistic dark matter component. In this paper we have employed a vast collection of recently available data, from Supernovae Ia to cosmic chronometers, from lensing to redshift space distortions, to estimate the anisotropic stress through the statistics η_{obs} , proposed in [16], that is independent of assumptions about background cosmology, galaxy bias, initial conditions, and matter abundance.

Since the current datasets have been obtained at different redshifts, and because η_{obs} requires derivatives of data points, we need to interpolate the data in order to build η_{obs} . We adopted three different strategies to do so: binning, Gaussian Process, and polynomial regression. The Gaussian Process makes the strongest assumption, reducing the uncertainty to a very small number of parameters. Indeed, the Gaussian Process method delivers the

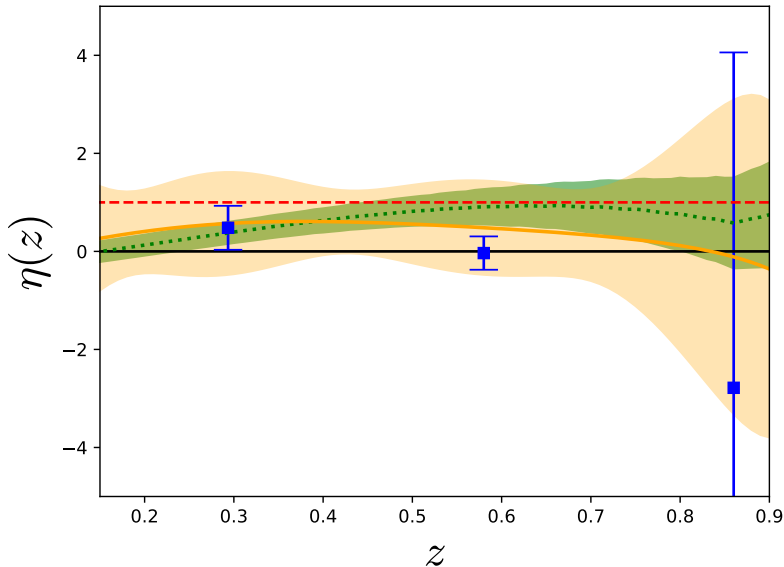


Figure 3. Plot of the reconstructed η_{obs} as a function of redshift, using the binning method (blue squares), Gaussian Process (green dotted line) and polynomial regression (yellow solid line). The corresponding error bands (error bars for the binning method), represent the 1σ estimated error on the reconstruction. As a reference, we show in a dashed red line the value in standard gravity.

most stringent error bars. The polynomial regression method employs free polynomials in which the order is given by the quality and quantity of data points (up to sixth order, in our case) to fit the data and evaluate the derivatives at the required points.

We find that the results are compatible with each other for the first bin, where data are more abundant. In the second bin, the binning method is 1.5σ away from the GP. For the third and farthest bin, the errors are so large that the comparison is hardly significant. In some cases, the standard gravity value $\eta = 1$ is two or even three sigma away from our result, but it is in every bin compatible for at least two of the three methods.

We quote as our fiducial result the error bars produced by the polynomial regression method: we find $\eta_{\text{obs}} = 0.44 \pm 0.92$ at $z = 0.294$, $\eta_{\text{obs}} = 0.42 \pm 0.89$ at $z = 0.58$, and $\eta_{\text{obs}} = -0.14 \pm 3.01$ at $z = 0.86$. Assuming a constant η_{obs} in this range and performing a simple weighted average, we find finally $\eta_{\text{obs}} = 0.49 \pm 0.69$. We consider this as the most reliable and conservative result. The other two methods give for a constant anisotropic stress $\eta_{\text{obs}} = 0.15 \pm 0.27$ (binning) and $\eta_{\text{obs}} = 0.62 \pm 0.19$ (Gaussian Process).

Future surveys, such as the Euclid satellite, will soon produce very large datasets for all the relevant observables that enter η_{obs} . The forecasts produced in [14] show that a constant η_{obs} could be measured up to a few percent. This is an exciting prospect, if one compares it to the 100% (or larger) error bars we find for the present observations.

Acknowledgments

A.M.P. gratefully acknowledges the support by the Landesgraduiertenförderung (LGF) grant of the Graduiertenakademie Universität Heidelberg. S.C. acknowledges support from CNRS and CNES grants. We acknowledge support from DFG through project TR33 “The Dark

Table 3. $H(z)$ measurements compiled by [23] with the respective original references.

z	$H(z)$ (km/s/Mpc)	$\sigma_{H(z)}$ (km/s/Mpc)	Reference	Method	z	$H(z)$ (km/s/Mpc)	$\sigma_{H(z)}$ (km/s/Mpc)	Reference	Method
0.07	69	19.6	[41]	1	0.510	90.4	1.9	[42]	2
0.09	69	12	[34]	1	0.593	104	13	[36]	1
0.12	68.6	26.2	[41]	1	0.600	87.9	6.1	[44]	2
0.17	83	8	[34]	1	0.610	97.3	2.1	[42]	1
0.179	75	4	[36]	1	0.680	92	8	[36]	1
0.199	75	5	[36]	1	0.730	97.3	7	[44]	2
0.2	72.9	29.6	[41]	1	0.781	105	12	[36]	1
0.27	77	14	[34]	1	0.875	125	17	[36]	1
0.28	88.8	36.6	[41]	1	0.880	90	40	[35]	1
0.352	83	14	[36]	1	0.900	117	23	[34]	1
0.38	81.5	1.9	[42]	2	1.037	154	20	[36]	1
0.3802	83	13.5	[40]	1	1.300	168	17	[34]	1
0.4	95	17	[34]	1	1.363	160	33.6	[37]	1
0.4004	77	10.2	[40]	1	1.430	177	18	[34]	1
0.4247	87.1	11.2	[40]	1	1.530	140	14	[34]	1
0.44	82.6	7.8	[44]	2	1.750	202	40	[34]	1
0.4497	92.8	12.9	[40]	1	1.965	186.5	50.4	[37]	1
0.4783	80.9	9	[40]	1	2.340	222	7	[38]	3
0.480	97	62	[35]	1	2.360	226	8	[39]	3

Table 4. $E(z)$ measurements from [43]. The error of the last measurement is not symmetric therefore it was recalculated as the quadrature of the 1σ bounds on the left and right side of the central value.

z	$E(z)$	$\sigma_{E(z)}$
0.07	0.997	0.023
0.2	1.111	0.020
0.35	1.128	0.037
0.55	1.364	0.063
0.9	1.52	0.12
1.5	2.67	0.675

Table 5. Covariance matrix for the $H(z)$ data from [42].

z	Covariance matrix		
0.38	3.65	1.78	0.93
0.51	1.78	3.65	2.20
0.61	0.93	2.20	4.45

Table 6. Covariance matrix for the $H(z)$ data from [44].

z	Covariance matrix		
0.44	0.0064	0.0025704	0
0.60	0.0025704	0.003969	0.00254016
0.73	0	0.00254016	0.005184

Universe”. We also acknowledge partial support from DAAD PPP Portugal bilateral project. We thank Adriá Gomez for useful discussions on the data analysis.

A The impact of the H_0 choice

Since our model-independent estimation for η requires the dimensionless Hubble function, that is $E(z) = H(z)/H_0$, we need to choose the value of H_0 to transform the $H(z)$ data into $E(z)$. However, there is a statistically significant tension between the values measured by different probes, namely the value from the 2018 results of the Planck collaboration [32] which is $H_0^{Planck} = 67.36 \pm 0.54$ [km/s/Mpc] and the value from HST collaboration [33] which

Table 7. Table of the $E_g(z)$ data set. The first column is the redshift, the second one is the value with the corresponding error on the third column. The fourth column shows the considered interval in real space that was used to obtain each data point and the last column points to the reference in the literature.

z	$E_g(z)$	$\sigma_{E_g(z)}$	Scale ($h^{-1}Mpc$)	Reference
0.267	0.43	0.13	$5 < R_p < 40$	[31]
0.305	0.27	0.08	$5 < R_p < 60$	[31]
0.32	0.40	0.09	$R_p > 3$	[45]
0.32	0.48	0.10	$R_p > 10$	[45]
0.554	0.26	0.07	$5 < R_p < 60$	[31]
0.57	0.31	0.06	$R_p > 3$	[45]
0.57	0.30	0.07	$R_p > 10$	[45]
0.60	0.16	0.09	$3 < R_p < 20$	[62]
0.86	0.09	0.07	$3 < R_p < 20$	[62]

Table 8. $f\sigma_8(z)$ data with the correspondent redshift and error. The fourth column points to the reference in literature.

z	$f\sigma_8(z)$	$\sigma_{f\sigma_8(z)}$	Reference	z	$f\sigma_8(z)$	$\sigma_{f\sigma_8(z)}$	Reference	z	$f\sigma_8(z)$	$\sigma_{f\sigma_8(z)}$	Reference
0.067	0.423	0.055	[46]	0.44	0.416	0.080	[44]	0.727	0.296	0.077	[49]
0.15	0.49	0.15	[52]	0.51	0.458	0.038	[42]	0.73	0.437	0.072	[44]
0.17	0.51	0.06	[48]	0.55	0.444	0.038	[56]	0.80	0.47	0.08	[50]
0.25	0.3512	0.0583	[53]	0.57	0.488	0.060	[57], [58]	0.85	0.45	0.11	[51]
0.30	0.366	0.067	[54]	0.60	0.390	0.063	[44]	0.86	0.46	0.09	[28]
0.35	0.445	0.097	[55]	0.60	0.441	0.071	[54]	0.86	0.48	0.10	[28]
0.37	0.4602	0.0378	[53]	0.60	0.48	0.11	[28]	1.36	0.482	0.116	[47]
0.38	0.497	0.045	[42]	0.60	0.48	0.12	[28]				
0.40	0.394	0.068	[56]	0.61	0.436	0.034	[42]				

is $H_0^{HST} = 73.45 \pm 1.66$ [km/s/Mpc]. Table 9 describes how the estimation of η shifts with the choice of H_0 . Generally the mean value and uncertainty do not significant change, as previously mentioned. However, for the last bin case, in particular for the binning case, the uncertainty increases for a factor of 10. While this result is compatible with the other bins, it shows how sensitive the binning method is. Since our aim is to have a model-independent estimation of η , we chose the HST collaboration H_0 value as it is approximately independent of a cosmological model.

Method	Choice of H_0	$\eta(z)$		
		$z_1 = 0.294$	$z_2 = 0.58$	$z_3 = 0.86$
Binning	H_0 HST	0.48 ± 0.45	-0.03 ± 0.34	-2.78 ± 6.84
	H_0 Planck 2018	0.56 ± 0.54	-0.14 ± 0.32	-6.75 ± 75.64
GaPP	H_0 HST	0.49 ± 0.25	0.94 ± 0.33	0.27 ± 0.67
	H_0 Planck 2018	0.31 ± 0.22	0.72 ± 0.33	0.36 ± 0.79
Linear Regression	H_0 HST	0.57 ± 1.05	0.48 ± 0.96	-0.11 ± 3.21
	H_0 Planck 2018	0.51 ± 1.07	0.37 ± 0.93	-0.18 ± 3.11

Table 9. The reconstructed $\eta(z)$ using different values of H_0 to normalize the $H(z)$ data at three different redshifts $z = (0.294, 0.58, 0.86)$ with its respective 1σ errors, for each of the reconstruction methods.

B Subtleties of the Gaussian Process method

We would like to note that the Gaussian Process method and the GaPP code are very sensitive to the dataset that one aims to reconstruct. Using the GaPP code which by default maximizes the hyperparameters, we have performed further tests with the $E(z)$ data, $f\sigma_8$ and $\ln(f\sigma_8(z))$.

In Section 5, we explained another approach to the usage of this code, where instead of letting the code determine the best-fit hyperparameters, we computed the logarithm of the marginal likelihood on a grid of hyperparameters and then we found the values that maximized it. This grid has 300 linear spaced values from 0.01 to 2 for σ_f and from 0.01 to the maximum reshift of the dataset for ℓ_f . For the $E(z)$ data, we find that there is no significant change but for the $f\sigma_8(z)$ and $\ln(f\sigma_8(z))$ data different reconstructions arise. For our work we used the $\ln(f\sigma_8(z))$ data, therefore we show in figure 4 the reconstructed function and its uncertainty band in green, together with the data used. On the left side, we see that GaPP estimates a best-fit correlation length of $\ell_f = 288$, which yields a very flat reconstruction of $\ln(f\sigma_8(z))$. On the right side of figure 4, we see that by setting a prior on the correlation length, that is from 0.01 to 1.36, we recover a function that follows much better the general data trend with $\ell_f = 1.36$ than the hyperparameters set by the GaPP optimization routine.

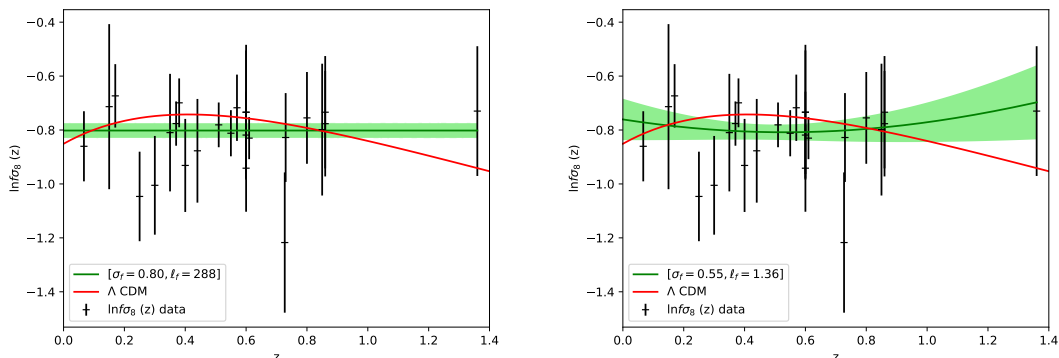


Figure 4. Reconstruction of the $\ln(f\sigma_8(z))$ data by the Gaussian Process method using the hyperparameters obtained by the GaPP code (left panel) and using a grid in hyperparameter space with a prior on ℓ_f (right panel).

C Details of the Polynomial Regression Method for the reconstruction of η_{obs}

We want to estimate the value of the functions $y^{(i)}$, for $i = 1, 2, 3, 4$ at a number of arbitrary points, labeled by subscripts $A, B, C \dots$, which we can call the interpolated points and assume that there is a domain \mathcal{D} common to all datasets, in which all the interpolated points are contained. We further assume that the three initial datasets, $y^{(j)}$, for $j = 0, 1, 2$ are

independent of each other. Now we use for all initial datasets, a polynomial of the form

$$g^{(j)} = \sum_{\alpha=0}^{N_j} (1+x)^\alpha \quad (\text{C.1})$$

with N_j the maximum order of the polynomial, which depends on the characteristics of each dataset $y^{(j)}$, and will be explained further below. Then the function f in Eq. (4.8) will have $N_j + 1$ coefficients, ranging from \bar{A}_0 to \bar{A}_{N_j} . If we now take the derivative of this function, we obtain

$$f^{(j)'} = \sum_{\mu=1}^{N_j} -\mu \bar{A}_\mu^{(j)} g_\mu^{(j)} = - \sum_{\mu=1}^{N_j} \bar{B}_\mu^{(j)} g_\mu^{(j)} \quad (\text{C.2})$$

where $g_\alpha^{(j)}$ is the α -th term in the sum $g^{(j)}$. For notational simplicity we define the indices α, β to always run from 0 to N_j , while the indices μ, ν will run from 1 to N_j . As we can see, the derivative functions $f^{(j)'}$ have one coefficient less, because there is no A_0 coefficient. The relation between the old and new coefficients is

$$\bar{B}_\mu = \mu \bar{A}_\mu \quad (\text{C.3})$$

This means that the covariance matrix $(F^j)^{-1}$ of the coefficients \bar{A}^j has to be modified with a Jacobian of the form

$$J_{\mu\alpha}^j = \frac{\partial \bar{B}_\mu}{\partial \bar{A}_\alpha} = \mu \delta_{\alpha\mu} = \text{diag}(0, 1, 2, \dots, N_j) \quad (\text{C.4})$$

to obtain the covariance matrix \tilde{F} of the new coefficients

$$(\tilde{F}^j)^{-1}_{\mu\nu} = J_{\mu\alpha}^j (F_{\alpha\beta}^j)^{-1} J_{\beta\nu} \quad . \quad (\text{C.5})$$

Since $\alpha, \beta = 0, \dots, N_j$ and $\mu, \nu = 1, \dots, N_j$ the Jacobian is a rectangular matrix of dimensions $(N_j - 1) \times N_j$, therefore the \tilde{F} matrices will have a dimension equal to the original F minus unity.

Summarizing, we will have the following four functions at the wanted points A

$$\bar{f}_A^{(a)} = \bar{B}_{\{\alpha,\mu\}}^{(a)} p_{A\{\alpha,\mu\}}^{(a)} \quad (\text{C.6})$$

Where due to the derivative, we will have the following basis functions,

$$p_\alpha^{(1)} = g_\alpha^{(1)} \quad p_\alpha^{(2)} = g_\alpha^{(2)} \quad p_\mu^{(3)} = -g_\mu^{(0)} \quad p_\mu^{(4)} = -g_\mu^{(1)} \quad (\text{C.7})$$

for $\alpha = 0, \dots, N_j$ and $\mu = 1, \dots, N_j$. Which in turn leads to a change in the vector of coefficients, such that they read now

$$\bar{B}_\alpha^{(1)} = \bar{A}_\alpha^{(1)} \quad \bar{B}_\alpha^{(2)} = \bar{A}_\alpha^{(2)} \quad \bar{B}_\mu^{(3)} = \mu \bar{A}_\mu^{(0)} \quad \bar{B}_\mu^{(4)} = \mu \bar{A}_\mu^{(1)} \quad . \quad (\text{C.8})$$

The Fisher matrices for $\bar{B}^{(1)}$ and $\bar{B}^{(2)}$, are $F^{(1)}$ and $F^{(2)}$, respectively. For $\bar{B}^{(3)}$ the Fisher matrix is $\tilde{F}^{(3)}$, while for $\bar{B}^{(4)}$ it is $\tilde{F}^{(4)}$. The \tilde{F} matrices have a dimension smaller by one unit than the original F .

$$C_{\alpha\beta}^{(1,1)} = \text{Var}(\bar{B}_\alpha^{(1)} \bar{B}_\beta^{(1)}) = \left(F^{(1)}\right)_{\alpha\beta}^{-1} \quad (\text{C.9})$$

$$C_{\alpha\beta}^{(2,2)} = \text{Var}(\bar{B}_\alpha^{(2)} \bar{B}_\beta^{(2)}) = \left(F^{(2)}\right)_{\alpha\beta}^{-1} \quad (\text{C.10})$$

$$C_{\mu\nu}^{(3,3)} = \text{Var}(\bar{B}_\mu^{(3)} \bar{B}_\nu^{(3)}) = \left(\tilde{F}^{(3)}\right)_{\mu\nu}^{-1} \quad (\text{C.11})$$

$$C_{\mu\nu}^{(4,4)} = \text{Var}(\bar{B}_\mu^{(4)} \bar{B}_\nu^{(4)}) = \left(\tilde{F}^{(4)}\right)_{\mu\nu}^{-1} \quad (\text{C.12})$$

$$C_{\alpha\beta}^{(1,4)} = \text{Var}(\bar{B}_\alpha^{(1)} \bar{B}_\beta^{(4)}) = \text{Var}(\bar{A}_\alpha^{(1)} \beta \bar{A}_\beta^{(1)}) = \left(F^{(1)}\right)_{\alpha\gamma}^{-1} J_{\gamma\beta} \quad (\text{C.13})$$

The full matrix $\mathcal{C}_{ab,AB}$ is our final result: the covariance matrix at any two different points x_A, x_B for any pairs of datasets $f^{(a)}, f^{(b)}$

$$\mathcal{C}_{ab,AB} = C_{\alpha\beta}^{(a,b)} p_{A\alpha}^{(a)} p_{B\beta}^{(b)} \quad (\text{C.14})$$

References

- [1] B. P. Abbott et al., *Gravitational Waves and Gamma-Rays from a Binary Neutron Star Merger: GW170817 and GRB 170817A*, *The Astrophysical Journal* **848** (2017) L13.
- [2] B. P. Abbott et al., *Search for Post-merger Gravitational Waves from the Remnant of the Binary Neutron Star Merger GW170817*, *The Astrophysical Journal* **851** (2017) L16.
- [3] A. Albert et al., *Search for High-energy Neutrinos from Binary Neutron Star Merger GW170817 with ANTARES, IceCube, and the Pierre Auger Observatory*, *The Astrophysical Journal* **850** (2017) L35.
- [4] B. P. Abbott, others (LIGO Scientific Collaboration and Virgo), *Estimating the Contribution of Dynamical Ejecta in the Kilonova Associated with GW170817*, *The Astrophysical Journal* **850** (2017) L39.
- [5] B. P. Abbott et al., *Multi-messenger Observations of a Binary Neutron Star Merger**, *The Astrophysical Journal Letters* **848** (2017) L12.
- [6] L. Lombriser and A. Taylor, *Breaking a dark degeneracy with gravitational waves*, *Journal of Cosmology and Astroparticle Physics* **3** (2016) 031 [1509.08458].
- [7] L. Lombriser and N. A. Lima, *Challenges to self-acceleration in modified gravity from gravitational waves and large-scale structure*, *Physics Letters B* **765** (2017) 382 [1602.07670].
- [8] J. M. Ezquiaga and M. Zumalacárregui, *Dark Energy After GW170817: Dead Ends and the Road Ahead*, *Physical Review Letters* **119** (2017) 251304.
- [9] J. Sakstein and B. Jain, *Implications of the Neutron Star Merger GW170817 for Cosmological Scalar-Tensor Theories*, *Physical Review Letters* **119** (2017) 251303.
- [10] P. Creminelli and F. Vernizzi, *Dark Energy after GW170817 and GRB170817A*, *Physical Review Letters* **119** (2017) 251302.
- [11] T. Baker et al., *Strong Constraints on Cosmological Gravity from GW170817 and GRB 170817A*, *Physical Review Letters* **119** (2017) 251301.
- [12] L. Amendola, M. Kunz, I. D. Saltas and I. Sawicki, *The fate of large-scale structure in modified gravity after GW170817 and GRB170817A*, *Phys. Rev. Lett.* **120** (2018) 131101 [1711.04825].
- [13] G. W. Horndeski, *Second-order scalar-tensor field equations in a four-dimensional space*, *International Journal of Theoretical Physics* **10** (1974) 363.

- [14] L. Amendola et al., *Model-independent constraints on the cosmological anisotropic stress*, [1311.4765](#).
- [15] F. Könnig et al., *Stable and unstable cosmological models in bimetric massive gravity*, *Physical Review D* **90** (2014) 124014 [[1407.4331](#)].
- [16] L. Amendola et al., *Observables and unobservables in dark energy cosmologies*, *Physics Review D* (2012) [[1210.0439](#)].
- [17] A. De Felice, T. Kobayashi and S. Tsujikawa, *Effective gravitational couplings for cosmological perturbations in the most general scalar-tensor theories with second-order field equations*, *Physics Letters B* **706** (2011) 123.
- [18] A. D. Felice and S. Tsujikawa, *Conditions for the cosmological viability of the most general scalar-tensor theories and their applications to extended Galileon dark energy models*, *Journal of Cosmology and Astroparticle Physics* **2012** (2012) 007.
- [19] H. Nersisyan, N. A. Lima and L. Amendola, *Gravitational wave speed: Implications for models without a mass scale*, [1801.06683](#).
- [20] M. Motta et al., *Probing dark energy through scale dependence*, *Physical Review D* **88** (2013) 124035.
- [21] C. D. Leonard, P. G. Ferreira and C. Heymans, *Testing gravity with $E-G$: mapping theory onto observations*, *Journal of Cosmology and Astroparticle Physics* (2015) [[1510.04287](#)].
- [22] M. Seikel, C. Clarkson and M. Smith, *Reconstruction of dark energy and expansion dynamics using Gaussian processes*, *Journal of Cosmology and Astroparticle Physics* (2012) [[1204.2832](#)].
- [23] H. Yu, B. Ratra and F.-Y. Wang, *Hubble Parameter and Baryon Acoustic Oscillation Measurement Constraints on the Hubble Constant, the Deviation from the Spatially-Flat Lambda cdm Model, The Deceleration-Acceleration Transition Redshift, and Spatial Curvature*, [1711.03437](#).
- [24] A. Gómez-Valent and L. Amendola, *H_0 from cosmic chronometers and Type Ia supernovae, with Gaussian Processes and the novel Weighted Polynomial Regression method*, [1802.01505](#).
- [25] F. Melia and M. K. Yennapureddy, *Model Selection Using Cosmic Chronometers with Gaussian Processes*, [1802.02255](#).
- [26] T. Holsclaw, U. Alam, B. Sanso, H. Lee, K. Heitmann, S. Habib et al., *Nonparametric Reconstruction of the Dark Energy Equation of State from Diverse Data Sets*, *Physical Review D* **84** (2011) 083501 [[1104.2041](#)].
- [27] V. Marra and D. Sapone, *Null tests of the standard model using the linear model formalism*, [1712.09676](#).
- [28] S. de la Torre et al., *The VIMOS Public Extragalactic Redshift Survey (VIPERS). Gravity test from the combination of redshift-space distortions and galaxy-galaxy lensing at $0.5 < z < 1.2$* , *Astron. Astrophys.* **608** (2017) A44 [[1612.05647](#)].
- [29] P. Zhang, M. Liguori, R. Bean and S. Dodelson, *Probing Gravity at Cosmological Scales by Measurements which Test the Relationship between Gravitational Lensing and Matter Overdensity*, *Physical Review Letters* **99** (2007) 141302.
- [30] M. Kunz, *Degeneracy between the dark components resulting from the fact that gravity only measures the total energy-momentum tensor*, *Physical Review D* **80** (2009) 123001.
- [31] A. Amon et al., *KiDS+2dFLenS+GAMA: Testing the cosmological model with the Eg statistic*, [1711.10999](#).
- [32] N. Planck Collaboration, Aghanim et al., *Planck 2018 results. VI. Cosmological parameters*, *ArXiv e-prints* (2018) [[1807.06209](#)].

- [33] A. G. Riess, S. Casertano, W. Yuan, L. Macri, J. Anderson, J. W. MacKenty et al., *New Parallaxes of Galactic Cepheids from Spatially Scanning the Hubble Space Telescope: Implications for the Hubble Constant*, *The Astrophysical Journal* **855** (2018) 136 [[1801.01120](#)].
- [34] J. Simon, L. Verde and R. Jimenez, *Constraints on the redshift dependence of the dark energy potential*, *Physics Review D* **71** (2004) [[0412269](#)].
- [35] D. Stern, R. Jimenez, L. Verde et al., *Cosmic Chronometers: Constraining the Equation of State of Dark Energy. II. A Spectroscopic Catalog of Red Galaxies in Galaxy Clusters*, [0907.3152](#).
- [36] M. Moresco et al., *Improved constraints on the expansion rate of the Universe up to z 1.1 from the spectroscopic evolution of cosmic chronometers*, *JCAP* **1208** (2012) 006 [[1201.3609](#)].
- [37] M. Moresco, *Raising the bar: new constraints on the Hubble parameter with cosmic chronometers at $z \sim 2$* , *Mon. Not. Roy. Astron. Soc.* **450** (2015) L16 [[1503.01116](#)].
- [38] BOSS collaboration, T. Delubac et al., *Baryon acoustic oscillations in the Ly α forest of BOSS DR11 quasars*, *Astron. Astrophys.* **574** (2015) A59 [[1404.1801](#)].
- [39] BOSS collaboration, A. Font-Ribera et al., *Quasar-Lyman α Forest Cross-Correlation from BOSS DR11 : Baryon Acoustic Oscillations*, *JCAP* **1405** (2014) 027 [[1311.1767](#)].
- [40] M. Moresco, L. Pozzetti, A. Cimatti, R. Jimenez, C. Maraston, L. Verde et al., *A 6% measurement of the Hubble parameter at $z \sim 0.45$: direct evidence of the epoch of cosmic re-acceleration*, *Journal of Cosmology and Astroparticle Physics* **5** (2016) 014 [[1601.01701](#)].
- [41] C. Zhang, H. Zhang, S. Yuan, S. Liu, T.-J. Zhang and Y.-C. Sun, *Four New Observational $H(z)$ Data From Luminous Red Galaxies of Sloan Digital Sky Survey Data Release Seven*, [1207.4541](#).
- [42] S. Alam, M. Ata, S. Bailey et al., *The clustering of galaxies in the completed SDSS-III Baryon Oscillation Spectroscopic Survey: cosmological analysis of the DR12 galaxy sample*, *Monthly Notices of the Royal Astronomical Society* (2016) [[1607.03155](#)].
- [43] A. G. Riess, S. A. Rodney, D. M. Scolnic et al., *Type Ia Supernova Distances at $z > 1.5$ from the Hubble Space Telescope Multi-Cycle Treasury Programs: The Early Expansion Rate*, [1710.00844](#).
- [44] C. Blake, S. Brough, M. Colless et al., *The WiggleZ Dark Energy Survey: joint measurements of the expansion and growth history at $z < 1$* , *Monthly Notices of the Royal Astronomical Society* **425** (2012) 405.
- [45] C. Blake, S. Joudaki, C. Heymans et al., *RCSLenS: Testing gravitational physics through the cross-correlation of weak lensing and large-scale structure*, *Monthly Notices of the Royal Astronomical Society* (2016) [[1507.03086](#)].
- [46] F. Beutler, M. Blake, C. and Colless et al., *The 6dF Galaxy Survey: $z=0$ measurements of the growth rate and σ_8* , *Monthly Notices of the Royal Astronomical Society* **423** (2012) 3430.
- [47] T. Okumura, C. Hikage, T. Totani et al., *The Subaru FMOS galaxy redshift survey (FastSound). IV. New constraint on gravity theory from redshift space distortions at $z = 1.4$* , *Publications of the Astronomical Society of Japan, Volume 68, Issue 3, id.38 24 pp.* **68** (2015) [[1511.08083](#)].
- [48] Y.-S. Song and W. J. Percival, *Reconstructing the history of structure formation using redshift distortions*, *Journal of Cosmology and Astroparticle Physics* (2008) [[0807.0810](#)].
- [49] A. J. Hawken, B. R. Granett, A. Iovino et al., *The VIMOS Public Extragalactic Redshift Survey: Measuring the growth rate of structure around cosmic voids*, *Astronomy & Astrophysics* **607** (2016) [[1611.07046](#)].

- [50] S. de la Torre, L. Guzzo, J. A. Peacock et al., *The VIMOS Public Extragalactic Redshift Survey (VIPERS). Galaxy clustering and redshift-space distortions at $z=0.8$ in the first data release*, *Astronomy & Astrophysics, Volume 557, id.A54, 19 pp.* **557** (2013) [[1303.2622](#)].
- [51] F. G. Mohammad, B. R. Granett, L. Guzzo et al., *The VIMOS Public Extragalactic Redshift Survey (VIPERS): An unbiased estimate of the growth rate of structure at $z = 0.85$ using the clustering of luminous blue galaxies*, **1708.00026**.
- [52] C. Howlett, A. J. Ross, L. Samushia, W. J. Percival and M. Manera, *The clustering of the SDSS main galaxy sample – II. Mock galaxy catalogues and a measurement of the growth of structure from redshift space distortions at $z = 0.15$* , *Monthly Notices of the Royal Astronomical Society* **449** (2015) 848.
- [53] L. Samushia, W. J. Percival and A. Raccanelli, *Interpreting large-scale redshift-space distortion measurements*, *Monthly Notices of the Royal Astronomical Society* **420** (2012) 2102.
- [54] R. Tojeiro et al., *The clustering of galaxies in the SDSS-III Baryon Oscillation Spectroscopic Survey: measuring structure growth using passive galaxies*, *Mon. Not. Roy. Astron. Soc.* **424** (2012) 2339 [[1203.6565](#)].
- [55] C.-H. Chuang and Y. Wang, *Modelling the anisotropic two-point galaxy correlation function on small scales and single-probe measurements of $H(z)$, $D_A(z)$ and $f(z)\sigma_8(z)$ from the Sloan Digital Sky Survey DR7 luminous red galaxies*, *Monthly Notices of the Royal Astronomical Society* **435** (2013) 255 [[1209.0210](#)].
- [56] H. Gil-Marín et al., *The clustering of galaxies in the SDSS-III Baryon Oscillation Spectroscopic Survey: RSD measurement from the LOS-dependent power spectrum of DR12 BOSS galaxies*, *Mon. Not. Roy. Astron. Soc.* **460** (2016) 4188 [[1509.06386](#)].
- [57] H. Gil-Marín, W. Percival, A. Cuesta et al., *The clustering of galaxies in the SDSS-III Baryon Oscillation Spectroscopic Survey: BAO measurement from the LOS-dependent power spectrum of DR12 BOSS galaxies*, *Monthly Notices of the Royal Astronomical Society* **460** (2016) 4210.
- [58] C. Chuang, F. Prada, M. Pellejero-Ibanez et al., *The clustering of galaxies in the SDSS-III Baryon Oscillation Spectroscopic Survey: single-probe measurements from CMASS anisotropic galaxy clustering*, *Monthly Notices of the Royal Astronomical Society* **461** (2016) .
- [59] A. Cabré and E. Gaztañaga, *Clustering of luminous red galaxies - I. Large-scale redshift-space distortions*, *Monthly Notices of the Royal Astronomical Society* **393** (2009) 1183.
- [60] L. Guzzo, M. Pierleoni, B. Meneux et al., *A test of the nature of cosmic acceleration using galaxy redshift distortions*, *Nature* **451** (2008) 541.
- [61] C. Rasmussen and C. Williams, *Gaussian Processes for Machine Learning*. MIT Press, 2006.
- [62] S. de la Torre, E. Jullo, C. Giocoli et al., *The VIMOS Public Extragalactic Redshift Survey (VIPERS). Gravity test from the combination of redshift-space distortions and galaxy-galaxy lensing at $0.5 < z < 1.2$* , eprint *arXiv:1612.05647* (2016) [[1612.05647](#)].